EFFECTS OF DIFFERENT NANO SIZE AND BULK WO_3 ENRICHED BY HDPE COMPOSITES ON ATTENUATION OF THE X-RAY NARROW SPECTRUM

by

Amro OBEID [1,2*], ***Hanna EL BALAA*** [2], ***Omar EL SAMAD*** [2], ***Zainab ALSAYED*** [1], ***Ramadan AWAD*** [1], ***and Mohamed S. BADAWI*** [1,3]

[1] Department of Physics, Faculty of Science, Beirut Arab University, Beirut, Lebanon
[2] Lebanese Atomic Energy Commission, National Council for Scientific Research, Beirut, Lebanon
[3] Physics Department, Faculty of Science, Alexandria University, Alexandria, Egypt

Scientific paper
https://doi.org/10.2298/NTRP2104315O

The X-rays of the narrow-spectrum N-series ranging from 40 kV to 150 kV were used to determine the radiation attenuation ability of a new category of a polymer composite fabricated for shielding purposes. High density polyethylene was synthesized through a compression molding technique, and incorporated with various filler amounts (10, 15, 25, and 35 wt.%) of bulk micro-sized WO_3 (Sample A), two WO_3 nanoparticles 45 nm (Sample B), and 24 nm (Sample C). The WO_3 filler was identified and characterized using X-ray diffraction and a transmission electron microscope. The mass distribution of the chemical elements of the synthesized composites was determined by energy dispersive X-ray analysis. The obtained results of the different attenuation parameters revealed that the particle size and weight fraction of WO_3 particles have an outstanding effect on the X-ray shielding ability of this composite. The experimental measurements of the mass attenuation coefficients were compared to the theoretical values tabulated in the NIST databases XCOM and FFAST. The mass attenuation coefficient was increased with the increment of WO_3 wt.% as well as with the decrease of the WO_3 particle size. This improvement in the attenuation parameters of the NP(C) composite suggests their promising applications in radiation protection at the diagnostic level.

Key words: high density polyethylene, WO_3 nanoparticle, mass attenuation coefficient, radiation protection

INTRODUCTION

The X-ray exposures resulting from radiological procedures constitute the largest part of the population exposure from artificial radiation. There is a great demand to control these doses and therefore to optimize the design and use of X-ray imaging systems [1]. In diagnostic radiology, the most complete specification of X-ray beams is determined by their spectral distribution. The X-ray spectrum usually consists of several narrow characteristic peaks on a continuous spectrum. The transition of electrons from outer to inner atomic orbits produces characteristic peaks, while the continuous X-ray spectrum is comprised of bremsstrahlung radiation covering a wide energy distribution [2]. A description of radiation qualities of X-ray beams is usually specified in terms of the X-ray tube voltage, total filtration, and first half value layer [1].

Radiation protection of the patients, as well as occupational safety of the staff, are of great interest during radiation exposure when conducting different procedures. The attempts to minimize the dose in high risk regions while preserving good image qualities is a great challenge for most researchers. In this context, designing proper, cost-effective, lightweight, and efficient materials to maintain proper radiation shielding is developed through the use of polymer composite materials [3, 4]. It has been confirmed in the literature before the radiation attenuation efficiency of polymer composite materials against different types of radiation using various types of polymers and fillers [5-9].

The use of polymer composite materials as radiation shielding against X-rays is still promising and developing. The high density polyethylene (HDPE) was chosen as a polymer base matrix due to its unique properties such as lightness, availability, and easy processing. Tungsten oxide WO_3 in both bulk and nano-size form was incorporated as a filler within HDPE. The WO_3 is considered a heavy element with potentially radiation shielding behavior [10]. Many studies were focused on the impact of adding micro and nano-size metal oxides specially WO_3 in the X-ray

* Corresponding author; e-mail: amrobeid@gmail.com

attenuation of the synthesized composites, such as studying the X-ray attenuation characterization of Bi_2O_3/PVA and WO_3/PVA nano-fiber mats with different filler loadings (0-40 wt.%) prepared by using the electro-spinning method [11]. The obtained results were compared at various X-ray energies (8.64-25.20 keV) using an X-ray fluorescent (XRF) unit. The resultant experiments revealed that the Bi_2O_3/PVA nano-fiber mat attained higher X-ray attenuation ability more than the WO_3/PVA nano-fiber mat for all filler loadings. In addition, the prepared WO_3 or Na_2WO_4 containing poly-dimethylsiloxane, tantalum (Ta), and tantalum oxide (Ta_2O_5) contained universal silicone (UNSI) composites with concentrations 10, 20, 30, 40, and 50 wt.% for radiation shielding. By using diagnostic X-ray tube voltages operated at 83 and 121 kV, the X-ray attenuation properties of the composites were studied. The obtained results within the energy interval of 68-87 keV showed that the composites containing Ta and W were more effective compared to pure lead [12].

The incorporated tungsten nanoparticles as filler into the room temperature vulcanizing silicon rubber $(SiOC_2H_6)_n$ matrix, where the fabricated composite was prepared with various wt.% up to 80 wt.% to study the soft X-ray shielding abilities. The results revealed that above 69.5 keV of photon energy, the obtained composite showed better absorbance of X-rays compared to lead-based composites [13]. The prepared dioctyl phthalate (DOP) oil and emulsion polyvinyl chloride (PVC) powder were mixed by nano- and micro-powders of WO_3 and Bi_2O_3 to fabricate a paste having the weight ratio of 20 % PVC, 20 % DOP, and 60 % nano- and micro-metals. The X-ray shielding properties of the fabricated prototypes were determined using a CBCT unit and dosimeter. The obtained results indicated that the nano-structured WO_3 prototype was nearly 34 % more efficient in attenuating radiation compared to the micro-structured WO_3 prototype [14]. The attenuation ability of composites containing micro-sized and nano-sized WO_3 was studied in the X-rays diagnostic energy range 40-100 kV by embedding them as fillers in emulsion polyvinyl chloride (EPVC). The results showed that the attenuation ability of nano-sized WO_3 containing shields was better compared to that of the micro-particle size [15].

Only some articles have been published concerning the establishment of reference X-ray beam qualities at Secondary Standard Dosimetry Laboratory (SSDL) [16-19]. Over the past years, the Lebanese SSDL provided radiation protection calibrations using the reference X-ray beam qualities recommended by the ISO 4037-1 standard (narrow-spectrum series: N-40 to N-200). In the present study, the X-ray narrow-spectrum series were used to investigate the radiation shielding efficiency for the prepared HDPE/WO_3 composites which was synthesized by adding different particle sizes of the filler WO_3 at various weight fractions (10, 15, 25, and 35 wt.%) by using the compression molding technique. The new category of the HDPE/WO_3 composite provides useful information about the proper WO_3 size and wt.%, which is required to enhance the radiation attenuation properties of the composite for further applications in the fields of radiation protection and radiation shielding.

MATERIALS AND METHODS

Materials

Commercial HDPE (Egyptene HD5403EA grade) supplied by SIDPEC (Sidi-Kerir Petrochemicals Company, Egypt), with a density of 0.955 gcm^{-3} and a melt flow index (MFI) of about 0.35 g per 10 min was used as a polymer matrix. Tungsten (VI) oxide (WO_3) in powder form with (purity 99 %, particle size 25 μm, MW = = 231.84 $gmol^{-1}$, and density of 7.16 gcm^{-3}) was purchased from Sigma-Aldrich (USA) and used without further purification.

The WO_3 nanoparticle preparation

The mechanical method designated by a high-energy planetary ball mill (Retsch, PM 100, Lebanon) in the dry state was used for the preparation of WO_3 NP. The ball milling process was performed in a 250 mL zirconium oxide grinding jar at room temperature under the following conditions:

- The ratio of the ball of powder weight is 10:1, the rotation speed is about 400 rounds per minute (rpm), and the break time of 1 minute.
- Two different milling times were applied as a specific amount of the bulk WO_3 was milled for 30 minutes with an interval function of 1 minute and another amount for 2 hours with an interval function of 5 minutes.
- The milled WO_3 at different milling times were characterized and based on the resultant size of NP achieved.
- The two milling times at 30 minutes and 120 minutes were identified as WO_3 NP(B) for 45 nm size and WO_3 NP(C) for 24 nm size, respectively.

Polymer composite synthesis

Composites with a filler weight fraction (10 %, 15 %, 25 %, and 35 %) of WO_3 Bulk(A), WO_3 NP(B), and WO_3 NP(C) were prepared using the compression molding technique. The sample category, name, and description are mentioned in tab. 1. The HDPE pellets were accurately weighed and poured in a two-roll mill mixer (XK400, Shandong, China) heated at about 170 °C for 15 minutes and at a speed of 40 rpm. Specific amounts of either WO_3 Bulk(A) or WO_3 NP(B)

Table 1. Sample category, name, and descriptions

Category	Sample name	Descriptions
HDPE	HDPE	Polymer without reinforcement
Polymer composites of WO_3 Bulk(A) [Pure tungsten oxide as received]	10 wt.% WO_3 Bulk(A)	HDPE reinforced with 10 wt.% of WO_3 Bulk(A)
	15 wt.% WO_3 Bulk(A)	HDPE reinforced with 15 wt.% of WO_3 Bulk(A)
	25 wt.% WO_3 Bulk(A)	HDPE reinforced with 25 wt.% of WO_3 Bulk(A)
	35 wt.% WO_3 Bulk(A)	HDPE reinforced with 35 wt.% of WO_3 Bulk(A)
Polymer composites of WO_3 NP(B) [Tungsten oxide milled for 30 min]	10 wt.% WO_3 NP(B)	HDPE reinforced with 10 wt.% of WO_3 NP(B)
	15 wt.% WO_3 NP(B)	HDPE reinforced with 15 wt.% of WO_3 NP(B)
	25 wt.% WO_3 NP(B)	HDPE reinforced with 25 wt.% of WO_3 NP(B)
	35 wt.% WO_3 NP(B)	HDPE reinforced with 35 wt.% of WO_3 NP(B)
Polymer composites of WO_3 NP(C) [Tungsten oxide milled for 120 min]	10 wt.% WO_3 NP(C)	HDPE reinforced with 10 wt.% of WO_3 NP(C)
	15 wt.% WO_3 NP(C)	HDPE reinforced with 15 wt.% of WO_3 NP(C)
	25 wt.% WO_3 NP(C)	HDPE reinforced with 25 wt.% of WO_3 NP(C)
	35 wt.% WO_3 NP(C)	HDPE reinforced with 35 wt.% of WO_3 NP(C)

and (C) were added to the mixing chamber after complete melting of the polymer matrix with continuous mixing for 10 minutes, to prevent their agglomeration. The prepared samples were shaken for 10 minutes to promote complete and homogeneous mixing. The samples were gathered and molded in a rectangular stainless steel mold (25 cm × 25 cm × 0.3 cm), layered Teflon was used to get a smooth surface. After that, the hot press was applied at 10 MPa and 170 °C for 10 minutes, the pressure was increased progressively to 20 MPa for another 10 minutes, the shaped composite sample was water-cooled gradually to ambient temperature at a rate (20 °C per minute). A pure HDPE sample was prepared without any WO_3 additive, five disc specimens of 8.3 cm in diameter were cut from each prepared sheet to investigate their radiation shielding characteristics against X-rays.

EXPERIMENTAL TECHNIQUES

The XRD analysis

The X-ray diffraction (XRD) patterns of bulk WO_3 and the prepared WO_3 nanoparticle samples were obtained by XRD (Bruker, D8 advance) using a Cu-k radiation source (λ = 0.154 nm) within a range of 20º 2θ 70º. The running conditions for the X-ray tube were 40 kV and 40 mA, recorded with an increment step of 0.02° and exposure time of 1 second. The reference for the peaks fitting was taken from the International Centre for Diffraction Data (ICDD) PDF-2/2013 database.

The TEM analysis

A transmission electron microscope, TEM, (JEOL, JEM-2100F) was used and operated at 200 kV to study the size of the prepared WO_3 nanoparticles. The sample powder was dispersed in ethanol with ultra-sonication by directly depositing one drop on a Cu grid.

The EDX analysis

The energy dispersive X-ray, EDX, analysis of the synthesized composites was observed using (JEOL, JCM-6000PLUS, Lebanon) operated under low vacuum, 15 kV PC-high and magnification order of 1500.

Measurements of X-ray attenuation coefficients

In SSDL in the Lebanese Atomic Energy Commission (LAEC), Beirut, Lebanon, the X-ray attenuation measurements were done using an X-ray Irradiator System (X80-225 kV) integrated by Hopewell Designs, Inc. The basic components of the system consist of an X-ray generator (COMET, XRP-225), a controller (COMET, XRG), and an X-ray tube (COMET, MXR-225). The generated X-rays were measured using a calibrated Radcal diagnostic detector (AGMS-DM+, USA) connected to a Radcal diagnostic dosimeter (Accu-Gold+ Touch, USA). The detector is a Solid State kV/dose multisensor for radiography, fluoroscopy, dental, and mammography X-rays with a minimal dose sensitivity of 80 nGy. The distance between the X-ray tube and the detector was set to 100 cm, the exposure was set at 10 mA and 30 s for the narrow X-ray beam qualities (N-series): N40, N60, N80, N100, N120, and N150 that is in conformance with ISO 4037-1 [20], and the criteria set in IEC 61267 standards [21]. The mean energies of these radiation qualities given in ISO 4037-1 are shown in tab. 2.

The X-ray irradiation system set-up

The set-up and geometry of the measurement system at SSDL in LAEC are displayed in fig. 1.

The system consists of an X-ray irradiation room (I) and a separated control room (II) equipped with the following components and subcomponents: generator (1), cooler (2), X-ray housing (3), X-ray tube (4), shut-

Table 2. The ISO 4037-1 Narrow-Spectrum N-Series

X-ray N-Series	Effective energy [keV]	Total filtration [mm]			First HVL [mm]
		Al	Cu	Sn	
N-40	33	4	0.21	–	0.084
N-60	48	4	0.6	–	0.24
N-80	65	4	2.0	–	0.58
N-100	83	4	5.0	–	1.11
N-120	100	4	5.0	1.0	1.71
N-150	118	4	–	2.5	2.36

ter (5), aperture wheel holder (6), filter wheel holder (7), tube inherent permanent filter holder (8), sample holder (9), test samples (10), detector (11), irradiation platform (12), video color surveillance system (13), laser beam alignment (14), and remote controller to adjust the X-ray irradiation system (15). The initial dose was directly exposed to the detector without having any sample while the final dose was taken with the sample placed on the source-to-detector set-up, and repeated by adding five different samples of the same composite, consecutively. The linear attenuation coefficient μ [cm^{-1}], for each composite sample, was determined as the plotted slope of the linear relation between ln$D$ and x given by the following equation after the best fitting process.

$$\mu \quad \frac{1}{x} \ln \frac{D_0}{D_x} \tag{1}$$

where x is the thickness of disc specimens of the same composite sample in cm.

The apparent density, ρ, of each prepared composite sample was measured accurately by using a calibrated balance with a precision of 0.1 mg, and by applying the Archimedes' technique [22], using

$$\rho \quad \frac{A}{A \quad W \quad B} \rho_w \tag{2}$$

where A is the apparent mass of the specimen, without wire, weighed in air, B – the apparent mass of the specimen completely immersed and with wire partially immersed in water, W – the apparent mass of the partially immersed wire, and ρ_w – the density of water (1.00 g cm^{-3}). Then, the mass attenuation coefficient μ_m [cm^2 g^{-1}] is obtained by dividing μ by the measured density of the composite sample ρ as follows [23]

$$\mu_m \quad \frac{\mu}{\rho} \tag{3}$$

THEORETICAL VIEWPOINT

The theoretical values of the mass attenuation coefficients of the mixture or composite have been investigated by the NIST standard reference databases based on the mixture rule [24], assuming the contribution of each element to the total interaction of the X-ray photon.

The total mass attenuation coefficient is obtained by

$$\mu_m \quad {}_i \, w_i (\mu_m) \tag{4}$$

where w_i and $(\mu_m)_i$ represent the weight fraction and the mass attenuation coefficient of the constituent elements of the composite, respectively. While the weight faction w_i is defined as

$$w_i \quad \frac{n_i A_i}{{}_i \, n_i A_i} \tag{5}$$

where A_i and n_i are the atomic weight and the number of formula units of the ith constituent element of the composite, respectively.

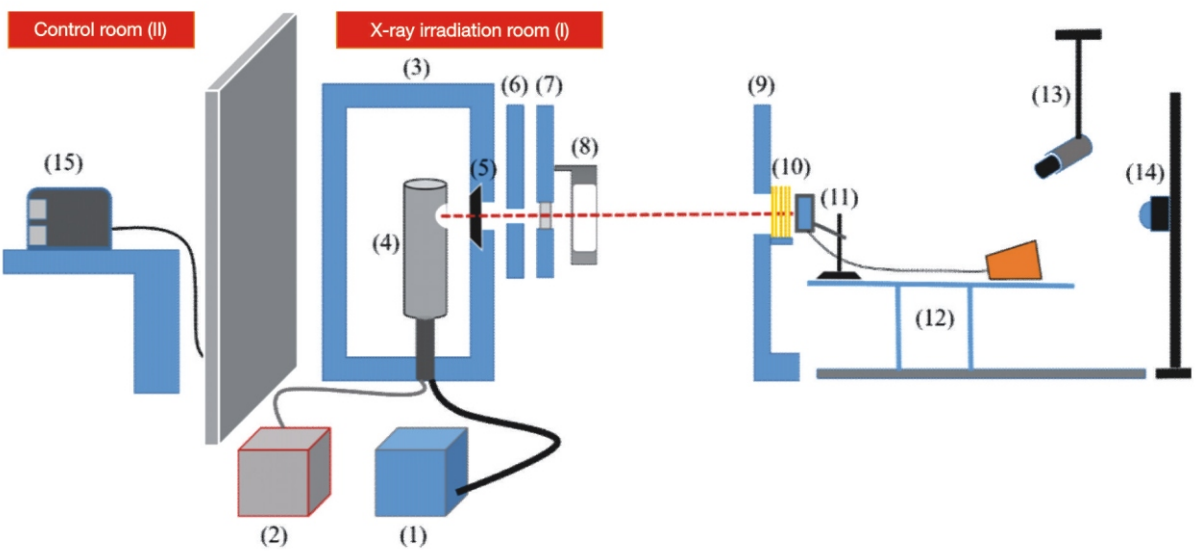

Figure 1. Diagram of the X-ray irradiation system set-up in the Lebanese SSDL

The theoretical values of density for the composites were calculated according to the [25]

$$\rho_T \quad \frac{100}{\frac{m_{\text{matrix}}}{\rho_m} \quad \frac{m_{\text{filler}}}{\rho_f}} \tag{6}$$

where m_{matrix} is the wt.% of HDPE, m_{filler} – the wt.% of WO_3, ρ_m – the density of HDPE, and ρ_f – the density of WO_3.

The experimental values obtained in this study were compared with the theoretical values evaluated from Berger's database, NIST XCOM, and Chantler's database, NIST FFAST. The half value layer HVL and tenth value layer TVL are described as the thickness of the radiation shielding material required to attenuate the intensity of radiation into 50 % and 10 % of its initial value, respectively. Both factors are given by

$$HVL \quad \frac{\ln 2}{\mu} \tag{7}$$

$$TVL \quad \frac{\ln 10}{\mu} \tag{8}$$

The relaxation length, λ, is the average distance between two successive interactions of photons (also known as the photon mean free path) can be computed by

$$\lambda \quad \frac{1}{\mu} \tag{9}$$

The heaviness of composites relative to pure lead was calculated as

$$\text{Heaviness} \quad \frac{\text{Density of composite}}{\text{Density of lead}} \quad 100\ [\%] \tag{10}$$

RESULTS AND DISCUSSION

The XRD patterns of the filler WO_3 Bulk(A), WO_3 NP(B), and WO_3 NP(C) are shown in fig. 2.

The diffraction peaks display nearly the same position with no tangible shift and are found to be highly matched with the ICDD (PDF file 01-083-0951), indicating the monoclinic structure of WO_3. The main diffraction peaks were found at 2θ values of 23.118°, 23.583°, 24.365°, 26.592°, 28.614°, 28.979°, 33.262°, 33.564°, and 34.166° corresponding to the planes (002), (020), (200), (120), (112), (121), (022), (202), and (220), respectively. The characteristic peaks of WO_3 Bulk(A) indicate high crystallinity due to the strength and sharpness of the peaks. The XRD patterns of WO_3 NP(B) and WO_3 NP(C) show the same peaks identical to WO_3 Bulk(A) with no shift in the position of the peaks. On the other hand, a clear broadening and a slight decrease in the intensity of the peaks are observed with the decrease of the nanoparticle size mainly for WO_3 NP(C) confirming

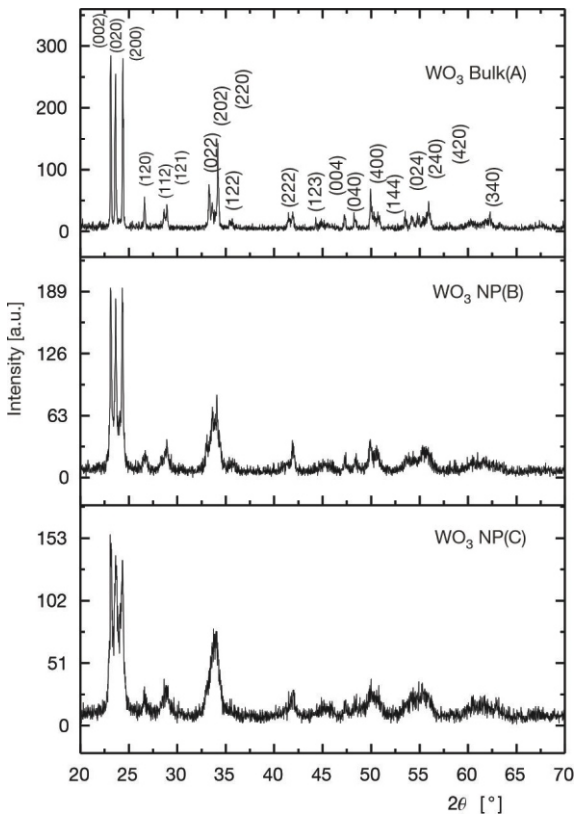

Figure 2. The XRD patterns of WO_3 Bulk(A), WO_3 NP(B), and WO_3 NP(C)

that the lowest degree of crystallinity is accompanied by the smaller crystalline size [26, 27].

The average crystallite size of the prepared WO_3 nanoparticles was determined by Scherrer's formula using the following relation [28]

$$D \quad \frac{0.9\lambda}{\beta \cos\theta} \tag{11}$$

where D is the average crystalline size, λ – the wavelength of Cu K , (λ = 1.5405 Å), β – the full width at half maximum (FWHM) intensity of the peak in radians, and 2θ – the Bragg's diffraction angle. The results are estimated at 45 nm for WO_3 NP(B) and 24 nm for WO_3 NP(C).

The TEM micrographs for the prepared WO_3 nanoparticles are described in figs. 3(a) and 3(b). The different particle size distribution based on the length scale provided in TEM images was measured using the Image software, where Gaussian distribution was performed. The average particle sizes obtained from TEM are 48 nm for WO_3 NP(B) and 27 nm for WO_3 NP(C). The results are approximately consistent with the average size extracted from XRD spectra. The energy dispersive X-ray analysis EDX was performed to detect the chemical elements for the synthesized HDPE composites WO_3 bulk(A), WO_3 NP(B), and NP(C), and the results are shown in tab. 3.

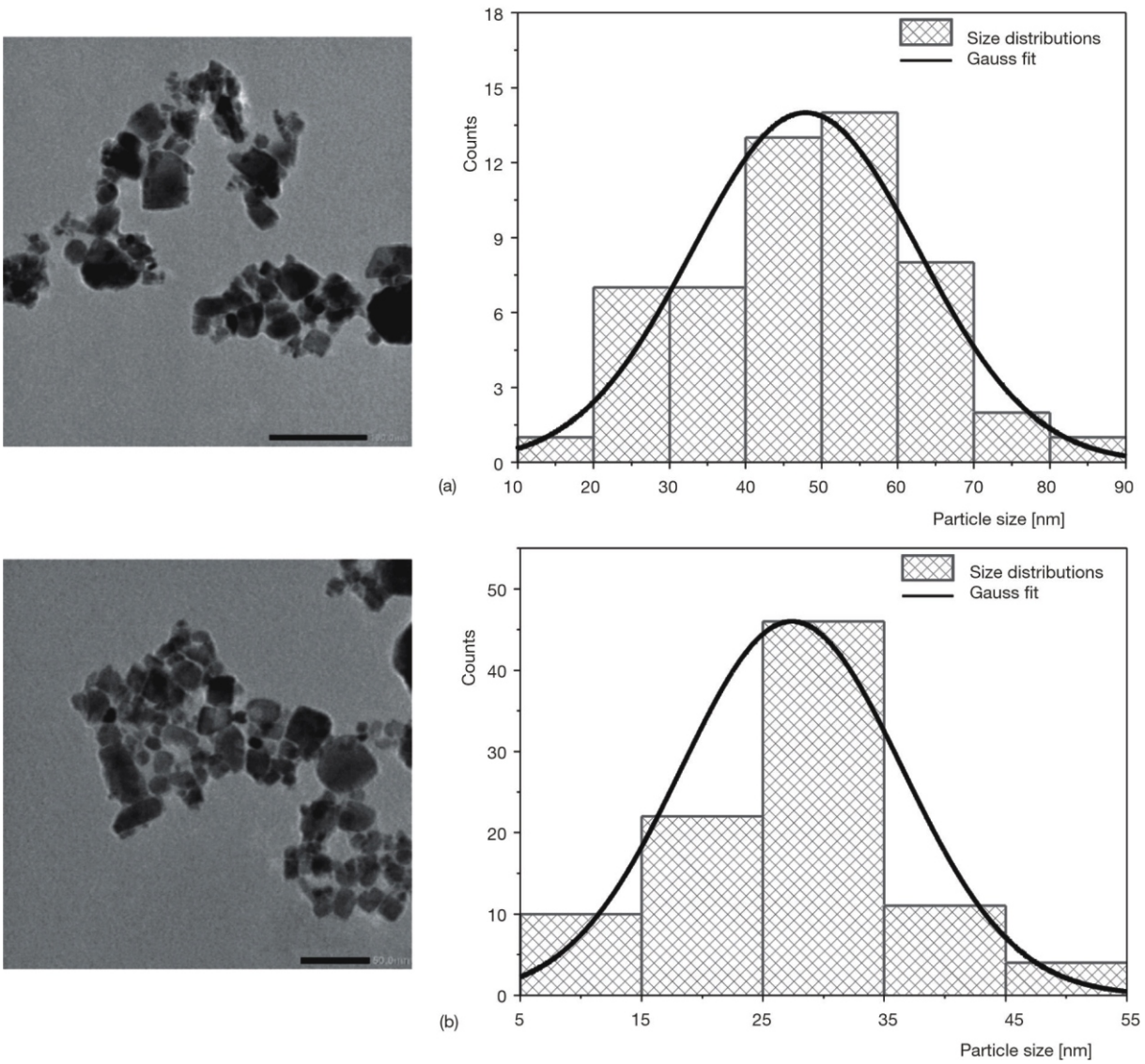

Figure 3. The TEM micrographs and particle size distribution of (a) WO_3 NP(B) and (b) WO_3 NP(C)

The C elements are mainly derived from the HDPE matrix. Furthermore, the EDX results show the existence of W elements from the filler in addition to Pt and Pd which were used as sputter coating for the specimen during the spectroscopy process. The presence of the oxygen peak is mainly attributed to the ionization caused by the electron beam path generated to interact with the specimen since a low vacuum is used as a condition for the EDX spectroscopy. A very weak peak of Al presents in the spectrum which could be attributed to the coating process and the specimen pedestal used during the spectroscopy process. The mass percentage of W appeared to increase to the lowest nanoparticle size indicating that WO_3 NP(C) occupies the largest surface of the quantitative analysis due to the large surface-to-volume ratio of the nanoparticles.

The density values calculated of HDPE/WO_3 composites using eqs. (2) and (6) are shown in tab. 4. The apparent densities for all samples increase with wt.% increment. The highest values are for the composite HDPE/WO_3 NP(C) compared to HDPE/WO_3 NP(B) and HDPE/WO_3 Bulk(A), respectively. The difference in density values is mainly attributed to a higher number of WO_3 fillers per gram for WO_3 NP *vs*. bulk WO_3 fillers. Furthermore, a significant difference can be noticed between the theoretical and experimental values of density in the samples having 35 wt.% of WO_3 filler due to their tendency towards the formation of voids at high filler loading [29].

The linear attenuation coefficient μ characterizes the probability of a photon being scattered or absorbed. Since the prepared samples have no uniform thickness and the concentration of electrons determined by the physical density of the samples are not in total agreement with the theoretical values as illustrated in tab. 4. Therefore, the use of the mass attenuation coefficient $\mu_m$is more convenient for comparing the X-ray attenuation capability of the prepared samples since it represents the fraction of photon interactions per unit mass per unit area [gcm^{-2}], producing a

Table 3. The EDX results for the chemical elements and mass distribution in all investigated HDPE composite samples

Sample description		Chemical elements and mass distribution [%]					
		Energy [keV]					
		0.277	1.774	2.048	2.838	0.525	1.486
		C	W	Pt	Pd	O	Al
HDPE/ WO_3 Bulk(A)	10 wt.%	58.49	0.25	33.94	2.91	3.77	0.63
	15 wt.%	71.06	0.35	23.69	2.10	2.37	0.43
	25 wt.%	47.54	0.39	44.78	4.29	2.05	0.96
	35 wt.%	63.17	3.95	27.15	2.42	2.84	0.47
HDPE/ WO_3 NP(B)	10 wt.%	67.23	1.53	25.81	2.36	2.55	0.51
	15 wt.%	66.35	2.71	24.67	2.24	3.58	0.45
	25 wt.%	62.44	4.38	28.00	2.46	2.22	0.50
	35 wt.%	54.74	8.31	31.35	2.73	2.26	0.60
HDPE/ WO_3 NP(C)	10 wt.%	59.15	2.83	31.90	3.01	2.57	0.54
	15 wt.%	59.25	3.11	31.43	2.89	2.64	0.68
	25 wt.%	62.56	6.47	25.16	2.31	2.99	0.52
	35 wt.%	55.77	8.50	30.11	2.64	2.47	0.50

Table 4. Theoretical and experimental density values for HDPE, HDPE/WO_3 Bulk(A), HDPE/WO_3 NP(B), and HDPE/WO_3 NP(C) composites at different wt.%

Sample type	Density values [gcm^{-3}]			
	Theoretical	Experimental		
HDPE	0.955	0.945 0.011		
–	–	WO_3 Bulk(A)	WO_3 NP(B)	WO_3 NP(C)
10 wt.%	1.045	1.009 0.025	1.019 0.021	1.039 0.012
15 wt.%	1.097	1.048 0.034	1.055 0.029	1.084 0.019
25 wt.%	1.219	1.156 0.044	1.178 ± 0.028	1.196 ± 0.015
35 wt.%	1.370	1.241 ± 0.091	1.273 ± 0.068	1.299 ± 0.050

constant value for a specific composite [30]. The measured values of the mass attenuation coefficient μ_m, the theoretical values of μ_m given by the NIST databases XCOM and FFAST, the discrepancy % between the measured and the theoretical values of $\mu_m$for HDPE and its composites Bulk(A), NP(B), and NP(C) at 33, 48, 65, 83, 100, and 118 keV, respectively are listed in tab. 5. It should be noted that in this study the X-ray narrow beam qualities of the ISO N-series were used, which explains the significant discrepancy values of some measurement NIST tabulations and experiment results by an amount of about 20 % at 65 keV and 83 keV in the region around the K-edge. Moreover, the database of NIST tabulations does not account for the size, structure, and density of the filler as well as the uniform dispersion of the filler within the polymer matrix. So, the attenuation coefficient values of composites in NIST are used as the advisory database only.

Many research groups reported the parameters that affect the emergence of significant discrepancies in their studies. The difference between experimental and theoretical values in discrepancies has been observed by Almeida Junior *et al*. [31], where the X-ray beam qualities of the ISO N-series were used and compared the obtained mass attenuation coefficients results to XCOM and FFAST for the same atomic composition which differ by more than 40 %. This was explained as an effect of the variations in the chemical composition of the samples and the nature of the mixing rule that neglects interactions between the atoms of the analyzed compounds. The difference in the experimental data of the relative response measured in the study of Massillon *et al*. [32] using X-ray beam qualities of the ISO N series and reported by Tedgren *et al*. [33] was about 6 % up to 15 %, where the phantom materials were similar. This was attributed to the dissimilarity of the energy spectra, and the geometrical conditions during the irradiation between the two experiments.

Figures 4(a)-4(c) illustrate the mass attenuation coefficient $\mu_m$of HDPE and its composites WO3 Bulk(A), WO_3 NP(B), and WO_3 NP(C) at various filler loadings as a function of X-ray energy, as listed in tab. 5. The values of the μ_m decrease as the X-ray energy increases from 33 up to 65 keV, then the same behavior is observed in the energy range from 83 up to 118 keV for all HDPE composites. The apparent spike between 65 and 83 keV is due to the K-edge absorption of W elements in the composite. For the X-ray energy range used in this experiment, the photoelectric effect represents the dominant contribution to the total interaction with the composite samples [34]. Usually, the photo-electrons move around and ionize one or more neighboring atoms together with the probability of emission of Auger electrons and fluorescent photons which leads to modifying the mass attenuation coefficient of the composite. As the energy increases, a more generated X-ray passes through the samples without interaction, and the occurrence of Compton scattering increases, leading to a decrease in the mass attenuation coefficient μ_m. The values of μm increase with the increment of WO_3 wt.% in the HDPE composites for all energies. This is due to the factor of a large number of WO_3 particles in the polymer matrix which increase the probability of X-ray interaction within the composite samples.

To compare the mass attenuation coefficients of different HDPE/WO_3 Bulk(A), WO_3 NP(B), and WO_3 NP(C) composites, a 3-D bar plot of μ_m with the color map was used in fig. 5 *vs*. X-ray energies at various WO_3 filler loadings. The particle size of the WO_3 filler has a significant effect on the value of μ_m which is higher at the same wt.% and energy for the WO_3 NP(C) composite compared to the WO_3 NP(B) composite and WO_3 Bulk(A) composite, respectively. The values of μ_m were increased with filler wt.% for all composites, while it was decreased with energy indicating the significant dependence of μ_m on both: the filler loading and energy values. In addition, for the same wt.% and at the same value of energy, the composites HDPE/WO_3 NP(C) show the highest value of μ_m compared to bulk composites and NP(B) compos-

Table 5. Measured and theoretical values of mass attenuation coefficients using the NIST databases XCOM and FFAST, and the discrepancy of HDPE, HDPE/WO_3 Bulk(A), HDPE/WO_3 NP(B), and HDPE/WO_3 NP(C) composites at various filler wt.% and different energies

Sample	Energy [keV]	Mass attenuation coefficient μ_m [cm^2g^{-1}]						
		Experimental value			XCOM	[%]	FFAST	[%]
HDPE	33	0.2110			0.2280	7.44	0.2506	15.76
	48	0.1881			0.1985	5.25	0.2201	14.54
	65	0.1693			0.1852	8.59	0.1982	14.56
	83	0.1604			0.1758	8.77	0.1821	11.90
	100	0.1559			0.1686	7.55	0.1708	8.70
	118	0.1427			0.1620	11.93	0.1613	11.53
Filler wt.%	Energy [keV]	Experimental value			XCOM	[%]	FFAST	[%]
		WO_3 Bulk(A)	WO_3 NP(B)	WO_3 NP(C)				
10 wt.%	33	1.4770	1.5281	1.7153	1.5289	3.39	1.6000	7.68
	48	0.6632	0.6698	0.7781	0.6599	0.50	0.7186	7.70
	65	0.4648	0.4806	0.52	0.3808	18.06	0.4164	10.41
	83	0.6414	0.6453	0.6855	0.7055	9.08	0.7102	9.68
	100	0.4355	0.4978	0.4996	0.4922	11.52	0.5012	13.09
	118	0.3675	0.3699	0.3743	0.3686	0.31	0.3779	2.75
15 wt.%	33	2.0100	2.2183	2.3186	2.1794	7.77	2.2748	11.64
	48	0.8736	0.9475	0.9555	0.8906	1.91	0.9678	9.73
	65	0.5807	0.6353	0.6413	0.4786	17.57	0.5255	9.50
	83	0.7799	0.8044	0.8095	0.9703	19.62	0.9743	9.95
	100	0.6077	0.6172	0.626	0.6540	7.09	0.6664	8.81
	118	0.4451	0.4582	0.46	0.4719	5.69	0.4862	8.45
25 wt.%	33	3.1300	3.1377	3.1482	3.4803	10.06	3.6242	13.63
	48	1.3676	1.3709	1.4913	1.3520	1.15	1.4662	6.72
	65	0.7038	0.7049	0.7392	0.6742	4.21	0.7438	5.36
	83	1.2278	1.2311	1.2332	1.4999	18.14	1.5024	18.27
	100	0.8975	0.9927	0.9938	0.9777	8.20	0.9968	9.96
	118	0.6664	0.6876	0.6824	0.6786	1.79	0.7028	5.17
35 wt.%	33	4.2118	4.4602	4.9578	4.7813	11.91	4.9737	15.32
	48	1.6699	1.7149	1.8329	1.8134	7.91	1.9647	15.01
	65	0.9193	1.0689	1.1225	0.8698	5.39	0.9620	4.43
	83	1.6464	1.6502	1.658	2.0296	18.88	2.0305	18.91
	100	1.1317	1.2111	1.2195	1.3013	13.03	1.3272	14.73
	118	0.8263	0.8477	0.8592	0.8852	6.65	0.9195	10.12

ites. Thus, the HDPE/WO_3 NP(C) composite may be considered a better potential X-ray shielding material candidate compared to the others. This is due to the nano-filler amplification in the composite, which increased its density, in addition to the high surface/volume ratio of nano-particles that increases the probability of X-ray interaction. In general, a material with high density is more effective for attenuating the primary X-ray beam since the probability of an X-ray interaction is relatively high due to tightly packed atoms inside [35]. Therefore, a good dispersion of the WO_3 NP filler even at high wt.% can be deduced from the result obtained.

The half value layer HVL, tenth value layer TVL and relaxation length, λ, are widely used parameters to study the radiation shielding properties of the composites. The calculated values of HVL, TVL, and λ for all HDPE/WO_3 composites, in addition to the HVL of pure lead, at different X-ray energies are given in tab. 6.

Based on the results found in tab. 6, the three parameters increase by increasing the X-ray energy from 33 to 65 keV. This behavior is followed by a slight decrease at 83 keV for all samples, then a significant increase is observed for higher energy values (100-118 keV). Since, HVL, TVL, and λ are inversely proportional to μ_m, the observed behavior of the three parameters along with the energy range is attributed to the alterations in the values of μ_m near the K-edge. It was noticed that, by increasing the wt.% of WO_3 of the composites, the values of HVL, TVL, and λ decrease, respectively, due to the increase of the mass attenuation coefficient and density. The HVL, TVL, and λ for HDPE/WO_3 Bulk(A), NP(B), and NP(C) composites *vs*. X-ray energy are displayed in figs. 6-8, respectively. It is found that the parameters of the NP(C) composite at the same filler loading wt.% exhibit lower values compared to NP(B) and Bulk(A) composites for all X-ray energies, which reflect the supe-

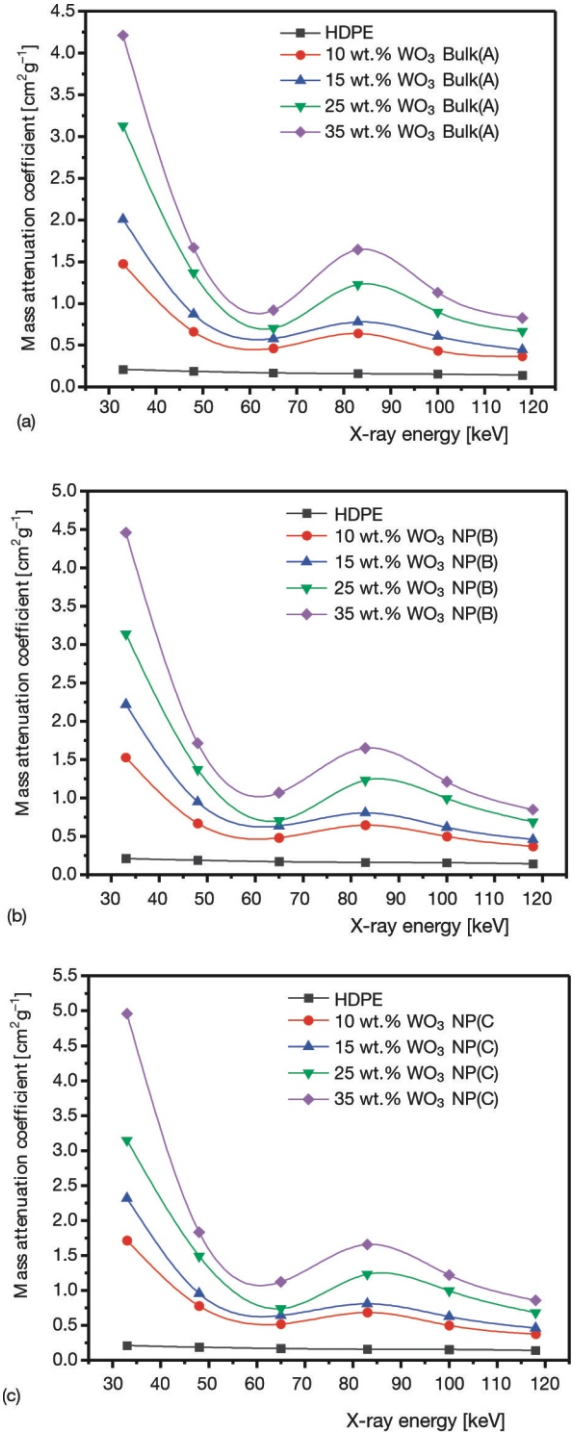

Figure 4. The mass attenuation coefficients versus X-ray energy of the HDPE (a) WO_3 Bulk(A) (b) WO_3 NP(B) (c) WO_3 NP(C) composite

rior shielding performance of the nanocomposites as compared to the synthesized bulk composites.

The HVL of pure lead as a conventional shielding material at the X-ray energy ranges from 33 to 118 keV is used for comparison with the investigated HDPE composites, and to clarify their effectiveness as radiation shielding materials. According to the results, the best lead equivalent appears at X-ray energy 83 keV, where a 3.216 mm thickness of the 35 wt.% HDPE/WO_3 NP(C) composite is equivalent to the 0.318 mm thickness of pure lead, which is 10.113 times the thickness of pure lead. Therefore, the composite with 35 wt.% of the smallest particle size WO_3 NP(C) represents a promising material selected to be used as an alternative radiation shielding material for X-ray diagnostic applications.

One of the most important parameters which must be taken into consideration when choosing a proper material for radiation shielding is the heaviness compared to lead. Polymer composites have become attractive materials for designing lightweight radiation shields. Figure 9 shows the percent heaviness of the HDPE/WO_3 composites by assuming pure lead as a reference and normalized to 100 %. The heaviness percent of HDPE is 8.33 %, while 35 wt.% of HDPE/WO_3 NP(C) is 11.45 % compared to pure lead. The synthesized polymer composites and even at high filler loading offer an efficient light matrix against radiation energy compared to a conventional lead shield.

CONCLUSION

The experimental results confirm the significant effect of the size and weight fraction of the WO_3 filler on the X-ray shielding ability of the new light, lead-free, and non-toxic HDPE/WO_3 polymer composites at all investigated X-ray narrow-spectrum beams (N40, N60, N80, N100, N120, and N150). The mass attenuation coefficient increases with the increment of WO_3 wt.% to the HDPE composite, which is more significant for the NP(C) composite compared to NP(B) and Bulk(A) composites for all X-ray energies. The nano-filler amplification in the polymer matrix results in high electron density, which increases the probability of the X-ray interaction within the nano-composites. The half value layer HVL, tenth value layer TVL and relaxation length λ decrease by increasing the wt.% of WO_3 in the composites. Moreover, the NP(C) composite at the same filler wt.% shows lower values of HVL, TVL, and λ compared to NP(B) and Bulk(A) composites for all X-ray energies. In addition, the sample with 35 wt.% HDPE/WO_3 NP(C) exhibits the best HVL compared to lead at X-ray energy 83 keV. The heaviness percentage of the HDPE/WO_3 composites by assuming pure lead as a reference even at high filler loading offers an efficient light matrix compared to the conventional lead radiation shield. Further, the radiation shielding performance of the polymer composites has superior factors compared to conventional lead including conformability, non-toxicity, cost-effectiveness, in addition to its remarkable improvement in mechanical properties because of the thermoplastic nature of the HDPE polymer matrix. Depending on the obtained results, the HDPE composite filled with WO_3 NP(C) can be considered as a promising novel alternative shielding material to be used in X-ray diagnostic applications.

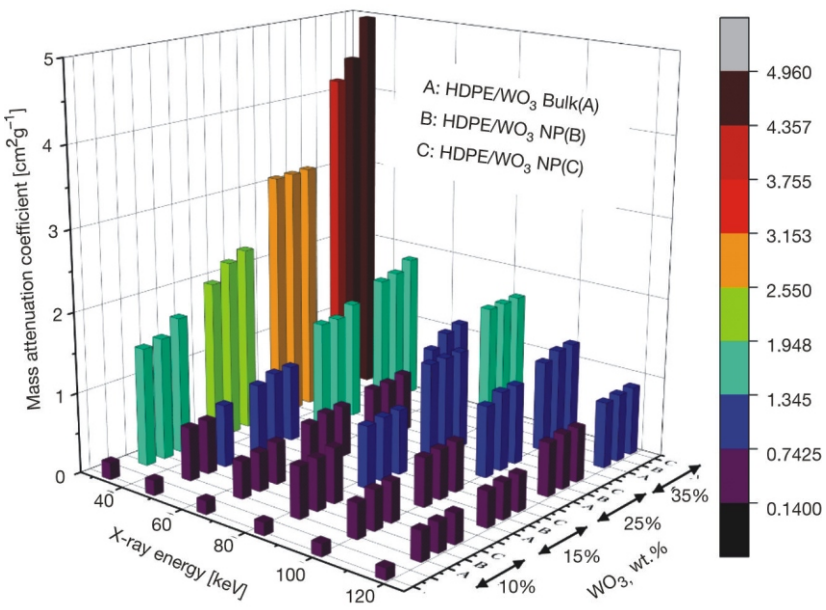

Figure 5. The comparison between mass attenuation coefficients of the HDPE/WO_3 Bulk(A), HDPE/WO_3 NP(B) and HDPE/WO_3 NP(C) composite of various WO_3 wt.% *vs*. X-ray energy

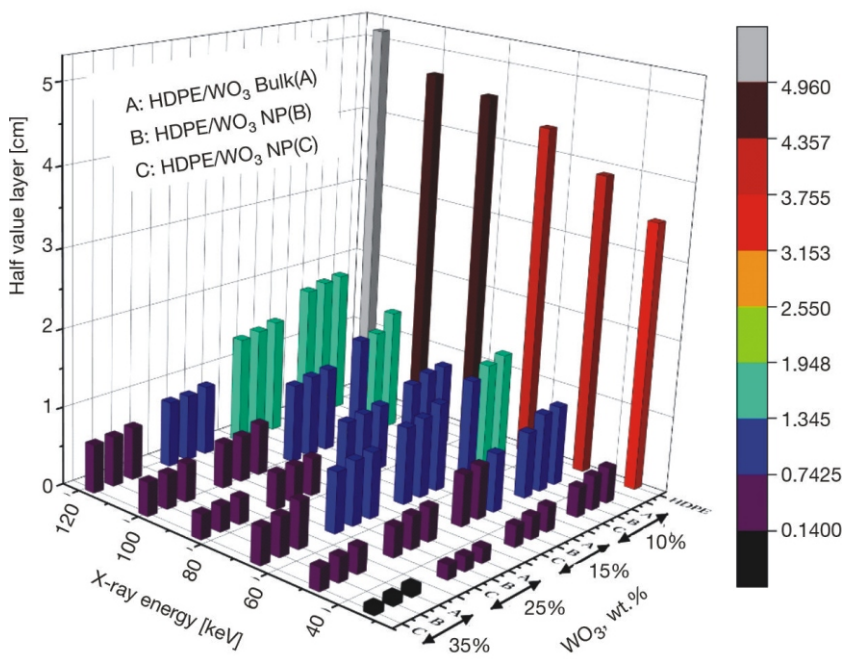

Figure 6. The HVL values of the HDPE/WO_3 Bulk(A) composite, HDPE/WO_3 NP(B) composite, and HDPE/WO_3 NP(C) composite of various WO_3 wt.% *vs*. X-ray energy

ACKNOWLEDGMENT

This work was done in the frame of the scientific collaboration between the Physics Department, Faculty of Science, Beirut Arab University (BAU), and the National Council for Scientific Research-Lebanon (CNRSL), Lebanese Atomic Energy Commission (LAEC). The main author would like to thank Mr. Malek Tabbal, Professor of Physics at the American University of Beirut (AUB), and the laboratory staff at KAS CRSL-AUB, for XRD and their valuable support.

AUTHORS' CONTRIBUTIONS

A. Obeid performed the experimental part with the valuable supervision of M. S. Badawi and H. El Balaa. M. S. Badawi, R. Awad, A. Obeid, and Z. Alsayed carried out the theoretical analysis and numerical testing performance. M. S. Badawi and A. Obeid drew and arranged all the figures. All authors reviewed and discussed the manuscript.

Table 6. Measured values of HVL, TVL, and λ of HDPE, HDPE/WO_3 Bulk(A), HDPE/WO_3 NP(B), and HDPE/WO_3 NP(C) composites in addition to the HVL of pure lead at different energies

Sample	Energy [keV]	HVL [cm]			TVL [cm]			λ [cm]		
HDPE	33	3.4713			11.5316			5.0081		
	48	3.8953			12.9400			5.6197		
	65	4.3267			14.3731			6.2421		
	83	4.5661			15.1685			6.5875		
	100	4.6993			15.6107			6.7796		
	118	5.1344			17.0561			7.4074		
Filler wt.%	Energy [keV]	HVL [cm]			TVL [cm]			[cm]		
		WO_3 Bulk(A)	WO_3 NP(B)	WO_3 NP(C)	WO_3 Bulk(A)	WO_3 NP(B)	WO_3 NP(C)	WO_3 Bulk(A)	WO_3 NP(B)	WO_3 NP(C)
10 wt.%	33	0.4649	0.44492	0.3888	1.5443	1.4780	1.2917	0.6707	0.6418	0.5610
	48	1.0353	1.01500	0.8572	3.4392	3.3717	2.8476	1.4936	1.4643	1.2367
	65	1.4772	1.41458	1.2826	4.9074	4.6991	4.2608	2.1312	2.0408	1.8504
	83	1.0704	1.05357	0.9730	3.5560	3.4999	3.2324	1.5443	1.5199	1.4038
	100	1.5764	1.36580	1.3350	5.2367	4.5371	4.4348	2.2742	1.9704	1.9260
	118	1.8683	1.83807	1.7818	6.2064	6.1059	5.9192	2.6954	2.6517	2.5706
15 wt.%	33	0.3288	0.2960	0.2755	1.0923	0.9834	0.9155	0.4744	0.4271	0.3976
	48	0.7565	0.6930	0.6687	2.5132	2.3023	2.2215	1.0914	0.9999	0.9647
	65	1.1381	1.0336	0.9963	3.7809	3.4336	3.3097	1.6420	1.4912	1.4374
	83	0.8474	0.8164	0.7893	2.8152	2.7120	2.6222	1.2226	1.1778	1.1388
	100	1.0876	1.0640	1.0206	3.6130	3.5348	3.3905	1.5691	1.5351	1.4725
	118	1.4848	1.4330	1.3883	4.9327	4.7604	4.6119	2.1422	2.0674	2.0029
25 wt.%	33	0.1914	0.1874	0.1866	0.6358	0.6226	0.6201	0.2761	0.2704	0.2693
	48	0.4381	0.4290	0.3883	1.4553	1.4251	1.2899	0.6320	0.6189	0.5602
	65	0.8512	0.8343	0.7833	2.8277	2.7715	2.6023	1.2280	1.2036	1.1301
	83	0.4880	0.4776	0.4696	1.6211	1.5868	1.5599	0.7040	0.6891	0.6774
	100	0.6675	0.5923	0.5827	2.2176	1.9676	1.9357	0.9631	0.8545	0.8406
	118	0.8990	0.8553	0.8485	2.9864	2.8414	2.8189	1.2970	1.2340	1.2242
35 wt.%	33	0.1326	0.1220	0.1075	0.4405	0.4054	0.3572	0.1913	0.1760	0.1551
	48	0.3344	0.3174	0.2909	1.1110	1.0545	0.9664	0.4825	0.4579	0.4197
	65	0.6075	0.5093	0.4750	2.0180	1.6919	1.5779	0.8764	0.7347	0.6853
	83	0.3392	0.3298	0.3216	1.1269	1.0958	1.0683	0.4894	0.4759	0.4639
	100	0.4935	0.4494	0.4372	1.6393	1.4931	1.4525	0.7119	0.6484	0.6308
	118	0.6758	0.6421	0.6205	2.2452	2.1331	2.0615	0.9750	0.9264	0.8953
Sample	Energy [keV]	HVL [cm]								
Pure lead (Pb)	33	0.0027								
	48	0.0074								
	65	0.0167								
	83	0.0318								
	100	0.0114								
	118	0.0174								

REFERENCES

[1] ***, Dosimetry in Diagnostic Radiology: An International Code of Practice, International Atomic Energy Agency, Vienna, 2007, p. 359

[2] Mincong, C., *et al*., An Examination of Mass Thickness Measurements with X-Ray Sources, *Applied Radiation and Isotopes, 66* (2008), 10, pp. 1387-1391

[3] Fontainha, C. C. P., *et al*., (VDF-TrFE)/ZrO_2 Polymer-Composites for X-Ray Shielding, *Materials Research, 19* (2016), 2, pp. 426-433

[4] Abbas, Y. M., *et al*., Gamma Attenuation Through Nano Lead - Nano Copper PVC Composites, *Nucl Technol Radiat, 36* (2021), 1, pp. 50-59

[5] More, C.V., *et al*., Polymeric Composite Materials for Radiation Shielding: A Review, *Environ. Chem. Lett., 19* (2021), Feb., pp. 2057-2090

[6] Alsayed, Z., *et al*., Study of Some Gamma Ray Attenuation Parameters for New Shielding Materials Composed of Nano ZnO Blended with High Density Polyethylene, *Nucl Technol Radiat, 34* (2019), 4, pp. 342-352

[7] El-Khatib, A. M., *et al*., Author Correction, Gamma Attenuation Coefficients of Nano Cadmium Oxide/High Density Polyethylene Composites, *Scientific Reports, 11* (2021), Apr., p. 8135

[8] Alharshan, G. A., *et al*., A Comparative Study Between Nano Cadmium Oxide And Lead Oxide Rein-

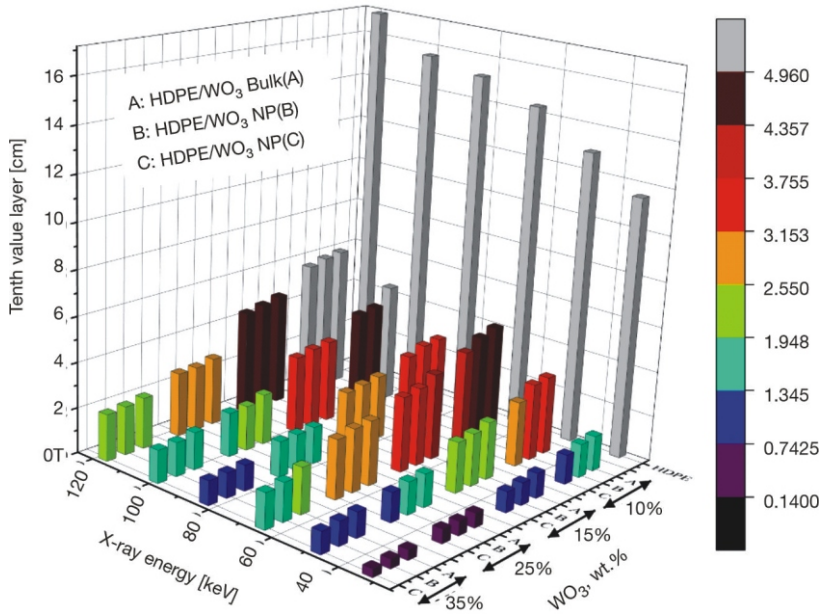

Figure 7. The TVL values of the HDPE/WO_3 Bulk(A) composite, HDPE/WO_3 NP(B) composite, and HDPE/WO_3 NP(C) composite of various WO_3 wt.% *vs*. X-ray energy

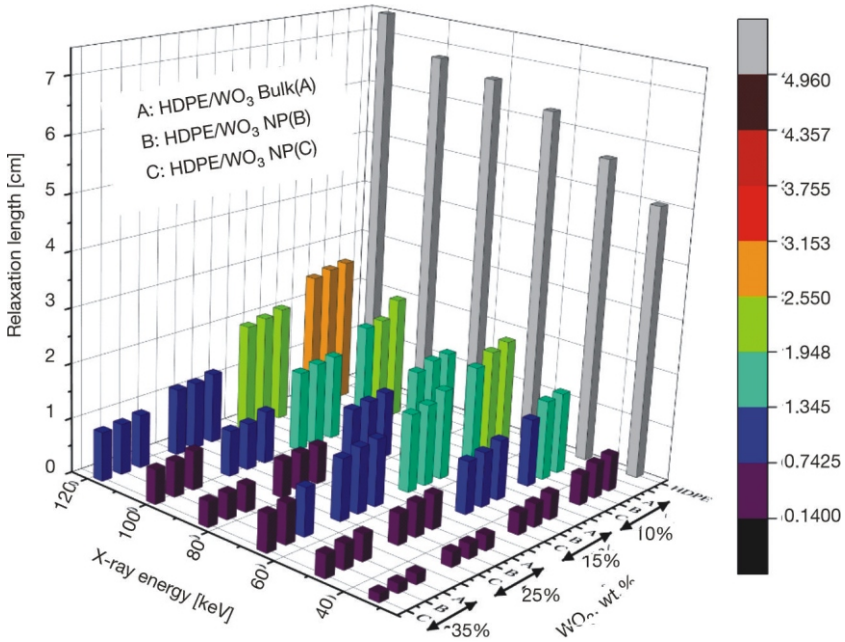

Figure 8. Relaxation length values of the HDPE/WO_3Bulk(A) composite, HDPE/WO_3 NP(B) composite, and HDPE/WO_3 NP(C) composite of various WO_3 wt.% *vs*. X-ray energy

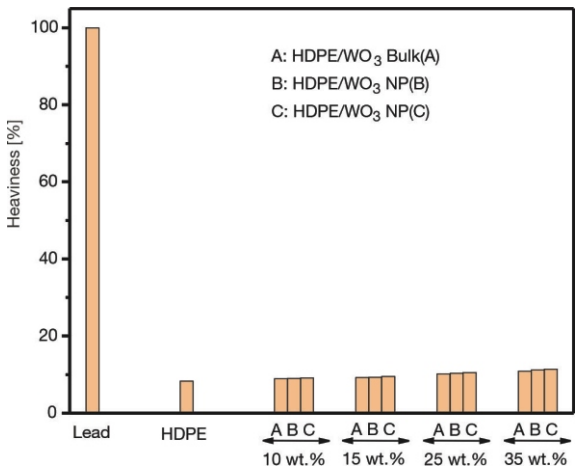

Figure 9. Heaviness percentage values of HDPE and HDPE/WO_3 composites compared to lead as a reference

forced in high Density Polyethylene as γ-Rays Shielding Composites, *Nucl Technol Radiat, 35* (2020), 1, pp. 42-49

[9] More, C. V., *et al*., Extensive Theoretical Study of Gamma-Ray Shielding Parameters Using Epoxy Resin-Metal Chloride Mixtures, *Nucl Technol Radiat, 35* (2020), 2, pp. 138-149

[10] Gavrish, V., *et al*., Investigations of the Influence of Tungsten Carbide and Tungsten Oxide Nanopowders on the Radiation Protection Properties of Cement Matrix-Based Composite Materials, *Journal of Physics Conference Series, 1652* (2020), Oct., p. 012008

[11] Hazlan, M. H., *et al*., X-Ray Attenuation Characterisation of Electrospun Bi_2O_3/PVA and WO_3/PVA Nanofibre Mats as Potential X-Ray Shielding Materials, *Applied Physics, 124* (2018), 7, p. 497

[12] Adliene, D., *et al*., Development and Characterization of New Tungsten and Tantalum Containing Composites for Radiation Shielding in Medicine, *Nuclear Instruments and Methods in Physics Research Section B, 467* (2020), Mar., pp. 21-26

[13] Dejangah, M., *et al*., X-Ray Attenuation and Mechanical Properties of Tungsten-Silicone Rubber Nanocomposites, *Materials Research Express, 6* (2019), 8, 085045

[14] Nikeghbal, K., *et al*., Designing and fabricating Nano-Structured and Micro-Structured Radiation Shields for Protection Against CBCT Exposure, *Materials, 13* (2020), 19, p. 4371

[15] Asari, N., *et al*., Study the Attenuation Ability of the Composites Containing Micro-Size and Nano-Sized Tungsten Oxide and Lead Oxide as Diagnostic X-Ray Shields, *Iranian Journal of Radiation Safety and Measurement, 5* (2017), 3, pp. 15-22

[16] Melhem, N., *et al*., Characteristics of the Narrow Spectrum Beams Used in the Secondary Standard Dosimetry Laboratory at the Lebanese Atomic Energy Commission, *Radiation Protection Dosimetry, 175* (2017), 2, pp. 252-259

[17] Zhang, D., *et al*., Establishment of ISO 4037-1 X-Ray Narrow Spectrum Series, *J. Eng., 2019* (2019), 23, pp. 8858-8861

[18] Herrati, A., *et al*., Establishment of ISO 4037-1 X-Ray Narrow-Spectrum Series at SSDL of Algiers, *Radiation Protection Dosimetry, 174* (2017), 1, pp. 35-52

[19] Bandalo, V., *et al*., ISO 4037:2019 Validation of Radiation Qualities by Means of half value Layer and Hp (10) Dosimetry, *Radiation Protection Dosimetry, 187* (2019), 4, pp. 438-450

[20] ***, ISO4037-1: X and Gamma Reference Radiation for Calibrating Dosemeters and Doserate Meters and for Determining Their Response as a Function of Photon Energy Part1: Radiation Characteristics and Production Methods, International Organization for Standardization, Geneva, Switzerland, 1996, p. 42

[21] ***, IEC Report 61267: Medical Diagnostic X-Ray Equipment-Radiation Conditions for Use in the Determination of Characteristics, International Electrotechnical Commission, Geneva, Switzerland 1994, p. 59

[22] ***, ASTM D792-13: Standard Test Methods for Density and Specific Gravity (Relative Density) of Plastics by Displacement, Annual Book of ASTM Standards, West Conshohocken, 2014, pp. 6

[23] Badawi, M. S., A Numerical Simulation Method for Calculation of Linear Attenuation Coefficients of Unidentified Sample Materials In Routine γ-Ray Spectrometry, *Nucl Technol Radiat, 30* (2015), 4, pp. 249-259

[24] Lokhande R. M., *et al*., Gamma Radiation Shielding Characteristics of Various Spinel Ferrite Nanocrystals: A Combined Experimental and Theoretical Investigation, *RSC Adv., 11* (2021), 14, pp. 7925-7937

[25] Azman, N. Z. N., *et al*., Microstructural Design of Lead Oxide-Epoxy Composites for Radiation Shielding Purposes, *J. Appl. Polym. Sci., 128* (2013), 5, pp. 3213-3219

[26] Shakya, V., *et al*., Electrical and Optical Properties of ZnO-WO_3 Nanocomposite and its Application as a Solid-State Humidity Sensor, *Bull. Mater. Sci., 40* (2017), 2, pp. 253-262

[27] Chandra, S. R., *et al*., H2S Sensors Based on Tungsten Oxide Nanostructures, *Sensors and Actuators B: Chemical, 128* (2008), 2, pp. 488-493

[28] Elements of X-Ray Diffraction, Addison-Wesley Publishing Company, US, 1978, p. 555

[29] Ambika, M. R., *et al*., Thermal Resistance and Mechanical Stability of Tungsten Oxide Filled Polymer Composite Radiation Shields, *International Journal of Polymer Analysis and Characterization, 25* (2020), 6, pp. 431-443

[30] Obaid, S. S., *et al*., Attenuation Coefficients and Exposure Buildup Factor of Some Rocks for Gamma Ray Shielding Applications, *Radiation Physics and Chemistry, 148* (2018), July, pp. 86-94

[31] Almeida Junior, T. A., *et al*., Mass Attenuation Coefficients of X-Rays in Different Barite Concrete Used in Radiation Protection as Shielding Against Ionizing Radiation, *Radiation Physics and Chemistry, 140* (2017), Nov., pp. 349-354

[32] Massillon-JL, G., *et al*., Influence of Phantom Materials on the Energy Dependence of LiF:Mg,Ti Thermoluminescent Dosimeters Exposed to 20-300 kV Narrow X-Ray Spectra, ^{137}Cs and ^{60}Co Photons, *Physics in Medicine and Biology, 59* (2014), 15, pp. 4149-4166

[33] Tedgren, A. C., *et al*., Response of LiF:Mg,Ti Thermoluminescent Dosimeters at Photon Energies Relevant to the Dosimetry of Brachytherapy (<1 MeV), *Med. Phys., 38* (2011), 10, pp. 5539-5550

[34] Yu, H., *et al*., Impact of Photoelectric Effect on X-ray Density Logging and Its Correction, *Appl. Rad. Isot., 156* (2020), Feb., pp. 1-22

[35] Kim, S.-C., Analysis of Shielding Performance of Radiation-Shielding Materials According to Particle Size and Clustering Effects, *Appl. Sci., 11* (2021), 9, pp. 1-10

Received on November 12, 2021
Accepted on March 4, 2022

Амро ОБЕИД, Хана ЕЛБАЛА, Омар ЕЛСАМАД, Заинаб АЛСАЈЕД, Рамадан АВАД, Мохамед С. Бадави

ЕФЕКТИ РАЗЛИЧИТИХ НАНО ВЕЛИЧИНА И РАСУТОГ WO_3 ОБОГАЋЕНОГ КОМПОЗИТИМА ПОЛИЕТИЛЕНА ВИСОКЕ ГУСТИНЕ НА СЛАБЉЕЊЕ X-ЗРАЧЕЊА УСКОГ СПЕКТРА

Рендгенски зраци H-серије уског спектра у опсегу од 40 kV до 150 kV коришћени су да би се одредила способност слабљења зрачења нове категорије полимерних композита произведених за потребе заштите. Полиетилен високе густине синтетизован је техником моделовања пресовањем и уграђен је са различитим количинама испуне (10, 15, 25, и 35 тежинских процената) расутог WO_3 микро величине (узорак А) и два узорка WO_3 наночестица од 45 nm (узорак Б) и 24 nm (узорак Ц). Испуна WO_3 идентификована је и окарактерисана коришћењем рендгенске дифракције и трансмисионог електронског микроскопа. Расподела масе хемијских елемената синтетизованих композита одређена је енергетско дисперзивном рендгенском анализом. Добијени резултати различитих параметара слабљења открили су да величина честица и тежински удео WO_3 честица овог композита имају изузетан утицај на својства заштите од рендгенских зрачења. Експериментална мерења масених коефицијената слабљења упоредена су са теоретским вредностима датим у табелама NIST база података – XCOM и FFAST. Масени коефицијент слабљења повећавао се са повећањем WO_3 тежинског процента као и са смањењем величине WO_3 честица. Ово побољшање параметара слабљења нано честичних композита сугерише њихову изгледну примену у заштити од зрачења на дијагностичком нивоу.

Кључне речи: полиетилен велике густине, WO_3 наночестица, масени коефицијент слабљења, заштита од зрачења